

000  
001  
002  
003  
004  
005  
006  
007  
008  
009  
010  
011

## Abstract

We propose a novel approach for the matching of partial deformable shapes in 3D. Inspired by recent advances in 2D template matching techniques, our method relies on the concept of deformable diversity similarity(DDIS), extends and adapts it from an image to the 3D shape domain, and leverages the distinct behavior of this framework in different scales to achieve shape correspondences. We evaluate this framework on the SHREC16 partial matching of deformable shapes and show state of the art performance in achieving sparse correspondences.

## 1. Introduction

Shape correspondence is a fundamental and challenging problem in computer vision and graphics. It has usage in various applications such as transferring texture and animation. Shapes rarely, if ever manifest in only one pose. While rigid transformations between surfaces is a well researched topic with many adequate solutions, a more challenging problem arises when a shape is deformed non-rigidly, though approximately isometrically, a case all too common for people, animals and objects. Moreover, shape acquisition processes almost always lead to partiality of the scanned object. Occlusions arise from different angles of acquisition, which cause an object to occlude itself, or stem from other occluding objects. Faulty sensors and bad acquisition conditions may also contribute to a creation of missing or noisy data. All of these combined give rise to the challenging problem of partial correspondences, where a deformed and incomplete shape, has to be matched with its full version. The goal of this paper is to deal with this challenging problem.

While in a rigid setting the problem can be solved by RANSAC and ICP like approaches/cite, extending these to non-rigid case produces mediocre results due to an underlying assumption of small deformations. Early methods specialized for the non-rigid problem focused on minimization of intrinsic metric distortion[6, 26, ?] and regularity of parts[?, 4]. These methods all contain with them a global

Anonymous CVPR submission

Paper ID \*\*\*\*

assumption of isometry which holds only approximately, these tended to break down with it, and are also unable to handle extreme partiality. Another family of method is based on functional correspondence. These methods model correspondences as a linear operator of a known nature between a space of functions on manifolds, usually the eigenfunctions of the Laplace Beltrami operator[14, 12, 27, 17]. These methods have achieved state of the art results on various partial matching tasks in recent year, and produce dense correspondence maps, but are not parallelizable, and their reliance on intrinsic metrics makes them invariant to symmetry.

We take a different approach. We take advantage of the fact that while the isometric property tends to break over large distances, it usually holds approximately in limited environments. These also tend to suffer a lot less from boundary effects, especially when concentrated around the extremities of a shape. We can thus treat the problem of partial correspondences as matching of multiple templates, each smaller than the partial surface centered around shape landmarks.

We follow the approach of[25] which tackles template matching in 2D and use simple statistical assumptions on the nature of nearest neighbors between small patch descriptors, along with the assumption of small deformations in medium environments to obtain similarity scores between these partial shape templates and produce sparse matches. Though the number of our generated correspondences is small, they prove to be superior in quality not only to other sparse correspondence producing methods, but also to state of the art dense correspondences.

In summary, our contributions are:

- A non trivial extension of Deformable Diversity from 2 to 3 Dimensions.
- A modified DDIS similarity measure which is more well suited to handle matching of templates with a different number of points, and is refined at multiple scales.
- A novel multi-template matching approach to partial matching of deformable shapes which produces sparse

108 correspondences which are competitive with state of  
109 the art methods.  
110

111 The rest of the work is organized as follows: in section  
112 we go over related works in the field of shape analysis.  
113 Section 3 introduces our Deformable Diversity framework  
114 for 3D shape matching. Experiments and results are given  
115 in section 4, and the conclusions are in section 5. **2. What**  
116 **previous work suggested -key ideas and drawbacks**

- 117    3. Our key ideas
- 118    4. Our results
- 119    5. Major contributions
- 120    6. Roadmap

## 122 **2. Related work**

124 **Matching Of Surfaces** As a fundamental problem in  
125 computer graphics and vision, an extensive body of work  
126 have been done on the matching of surfaces. For the  
127 rigid setup an adequate solution exists. Iterative Closest  
128 Point(ICP)[1] algorithm, preceded by initial alignment[21]  
129 tackle partial matching successfully. Adapting this to the  
130 rigid setup however has proved to have limited success due  
131 to the alignment which is necessary, and thus is only fit for  
132 very small non-rigid deformation. In contrast, early non-  
133 rigid correspondence methods were designed to work in the  
134 scenarios of little to no partiality. The assumption of near  
135 isometry[6] has been used commonly. This assumption is  
136 usually broken in the partial setup. Recent works, which  
137 address the full correspondence problem[2, 13, 24, 28]  
138 manage to cope with distortion by using smarter optimization  
139 objectives, but use the assumption of a bijection between  
140 the shapes, and thus cannot handle significant partiality.  
141 Early works which were designed with partial matching  
142 in mind[4, 5] solved a combined optimization problem  
143 over the metric distortion and the regularity of corresponding  
144 parts. Following works relaxed the regularity requirement  
145 by allowing for sparse correspondence[26] and controlling  
146 the sparsity of which [18]. Other metric distortion  
147 based works[22, 23] minimized the distortion metric over  
148 the shape extremities by doing combinatorial search of least  
149 distortion matches and then densify while refining them in  
150 the process. In addition to only supplying sparse correspondences  
151 and having a high computational complexity, relying  
152 only on the intrinsic distortion metric makes these methods  
153 fail when boundary effects plays a significant role.

154 In[15] a bag of words point-wise descriptors on a part in  
155 conjunction with a constraint on area similarity and the regularity  
156 of the boundary length to produce correspondence less matching  
157 parts without point to point correspondences.

158 Another notable family of works are derived from functional  
159 correspondences. Introduced at[14] these assume that  
160 correspondences between spaces of functions on a manifold  
161 can be modeled as a linear operators, approximately diagno-

162 nal given a smart choice of functions, which, given a small  
163 set of known correspondences can be recovered. The original  
164 paper used the Laplace Beltrami eigenfunctions. Following  
165 works employed joint diagonalization of the Laplacian  
166 matrices to find an optimal basis, and[16] extended it  
167 to the setting where the order of the functions is unknown,  
168 by solving for permutation of correspondence as well. It  
169 has been shown in [11] that matrix completion can address  
170 non-isometry and mild partiality. A combination with heat  
171 kernels as a distortion metric[27] has been shown to be  
172 able to handle some partiality, given an initialization with  
173 sparse correspondences, but this relies heavily on obtaining  
174 good initial correspondences, and thus application to partial  
175 matching has only been shown as a proof of concept.

176 Recently [17] had proven that partiality induces a slanted  
177 diagonal structure in the correspondence matrix and found  
178 the Laplacian eigenfunctions from each basis which induces  
179 this structure. Current state of the art[12] uses this notion  
180 in conjunction with joint diagonalization. The main draw-  
181 back of this method, shared with other intrinsic methods, is  
182 its invariance to symmetries. In addition, using sequential  
183 optimization, the entire family of methods cannot be parallelized.

184 **3D Shape Descriptors** A fundamental building block in  
185 many shape analysis tasks are shape descriptors , these are  
186 mappings  $f_{\mathcal{M}} : \mathcal{M} \rightarrow \Re^q, f_{\mathcal{N}} : \mathcal{N} \rightarrow \Re^q$  which are con-  
187 structed in a way which embeds similar shapes close in a  
188 euclidean space of dimension  $q$ . Shape descriptors of the  
189 extrinsic variety such as PFH[20], SHOT and FPFH[19]  
190 which are usually calculated in euclidean space and are thus  
191 sensitive to non rigid deformations, but are generally better  
192 in discerning between symmetrical shapes, and are also  
193 more robust to noise, topology artifacts and boundaries. On  
194 the other hand intrinsic features such as Heat[7] and Wave  
195 Kernel signatures[3] are invariant under isometric transfor-  
196 mations, but are very sensitive to partiality and are unable  
197 to discern between symmetric parts.

198 **Template matching in 2D** Template matching in 2D is  
199 a well researched topic. Similarly to 3D objects are going  
200 complex deformations of pose, and are only seen partially  
201 depending on the camera point of view. Recently a series of  
202 works which use a very simplistic framework based on the  
203 statistical properties of nearest neighbors in low level fea-  
204 ture space had made good strides in tackling this complex  
205 task.

206 **Best Buddies Similarity** Great strides had been  
207 achieved in the field of 2D template matching. Best Buddies  
208 Similarity[9] is a simple framework which employs a statis-  
209 tical assumption in which between two windows containing  
210 the same template  $\mathcal{N}, \mathcal{M}$  patches maintain Bi Directional  
211 Similarity. That is - given a point  $n_i \in \mathcal{N}$  and a correspond-  
212 ing point  $m_i \in \mathcal{M}$  they should maintain a relationship of  
213 Bi-Directional Similarity - that is if  $NN_{\mathcal{M}}(n_i) = m_j$  then

216 on a matching template we should expect  $NN_{\mathcal{N}}(m_j) = n_i$ .  
 217 This led to a significant improvement in template matching.  
 218

219 **Deformable Diversity Similarity** Building upon the  
 220 above work, [25] added two additional and rather simple  
 221 assumptions. The first of which is that the diversity of Near-  
 222 est Neighbors between corresponding templates should be  
 223 high. This is actually a prerequisite to a high best buddies  
 224 similarity score and serves as a rough approximations. For  
 225 this end diversity is formally defined as:  
 226

$$DIS = c \cdot |\{n_i \in \mathcal{N} : \exists m_j \in \mathcal{M}, NN(m_j, \mathcal{N}) = n_i\}| \quad (1)$$

227 where  $|\cdot|$  denotes group size and  $c = 1/\min(|\mathcal{M}|, |\mathcal{N}|)$  is  
 228 a normalization factor. Between non corresponding win-  
 229 dows, indeed one should expect most points to have no real  
 230 corresponding point, and thus be mapped to a very and re-  
 231 mote nearest neighbors. On the other hand, regions contain-  
 232 ing matching objects are drawn from the same distribution,  
 233 thus the diversity of nearest neighbors should be high. To  
 234 accommodate this assumption not only did they rewarded  
 235 high diversity of nearest neighbors, but also penalized map-  
 236 ping to the same patch. To this end, another, a negative  
 237 diversity measure had been defined:  
 238

$$\kappa(n_i) = |\{m \in \mathcal{M} : NN^a(m, \mathcal{N}) = n_i\}| \quad (2)$$

239 With  $x_i^a$  denoting the appearance descriptor of point  $x_i$ .  
 240 Thus the contribution of being a nearest neighbor to a patch  
 241 with multiple nearest neighbors would become  $\exp(1 -$   
 242  $\kappa(NN^a(m_j, \mathcal{N}))$ ). A final observation made has been that  
 243 while non rigid deformations do occur, they should be re-  
 244 stricted, small, in real objects. With the distance on the  
 245 window pixel grid between 2 nearest neighbor points de-  
 246 fined as  $r_j = d(m_j^l, n_i^l)$  with  $x_i^l$  denoting the location of  $x_i$   
 247 relative to the center of the template, the final Deformable  
 248 Diversity Similarity formulation becomes:  
 249

$$DDIS = c \sum_{m_j \in \mathcal{M}} \frac{1}{1 + r_j} \cdot \exp(1 - \kappa(NN^a(m_j, \mathcal{N}))) \quad (3)$$

### 250 3. Deformable Diversity for Partial matching 251 of 3D surfaces

252 **1. Goal of this section** In this section we will describe  
 253 the Deformable Diversity framework for matching of de-  
 254 formable shapes, as we had adjusted it for the 3D setting.  
 255 The algorithm follows the ideas presented by [25], and ad-  
 256 justs them for the unique challenges posed by the 3D setting  
 257 in which information is sparser and of varying density, and  
 258 the scenario of partial shape correspondence in which the  
 259 part and the scene are of comparable area.

260 **2. Key ideas of the algorithm** As stated above, a lot of  
 261 the key ideas are similar to the 2D scenario - the feature  
 262 nearest neighbor field between a part and his transformed  
 263

264 version tends to give rise to a high diversity of matches. In  
 265 addition, correct corresponding points between a template  
 266 and a matching object should lie in nearby regions with  
 267 relation to some reference point on the template. We im-  
 268 prove upon these with the realization that while deforma-  
 269 tion should hold very roughly for the entire part, it tends to  
 270 hold better the closer we are to the reference point. This  
 271 gives rise to a framework in which instead of matching the  
 272 whole template at once, we break it into multiple tasks of  
 273 smaller template matching, effectively using DDIS as a mid  
 274 level psuedo-metric to describe part similarity. Finally we  
 275 employ a strategy of choosing extremities on the surface for  
 276 the central points of the mini templates. Picking these ex-  
 277 tremities together with the matching of mini templates tends  
 278 to both mitigate boundary effects, and pushes the size of the  
 279 object in the full shape and the partial shape to be more sim-  
 280 ilar. Finally, we observe that DDIS has different properties  
 281 at different scales and thus employ a multi-scale cascade to  
 282 take advantage of this fact.

283 **3. Overview of the algorithm (Preprocessing (normal es-  
 284 timation, FPFH), Finding the landmark points, computing  
 285 DDIS correspondence for pairs, computing correspondence  
 286 of surfaces) Include an image of this general overview.**

287 The outline of the algorithm is as follows: we first cal-  
 288 culate the nearest neighbor field between the full shape and  
 289 the part - we begin by calculating local point descriptors  
 290 and use ANN to find for each point  $m_i \in \mathcal{M}$  its most similar  
 291 point  $NN^S(m_i, \mathcal{N})$ . We then use an extremity locating al-  
 292 gorithm to find suitable mini template centers. for each of  
 293 those we extract a surface piece of a certain geodesic radius  
 294 around it to serve as the mini template. Then for each of  
 295 these templates we look for the most similar piece of surface  
 296 of a similar radius around each point on  $\mathcal{M}$ . We use DDIS  
 297 as a similarity measure between all pairs of mini templates.  
 298 The points whose surface patch maximize this function for  
 299 each mini template are then set as the corresponding points  
 300 to their centers.

301 **4. Road-map to the section** We will begin with a de-  
 302 scription of the changes made for the deformable diversity  
 303 framework as a result of moving from 2D to 3D. We will  
 304 then go over the specific stages of preprocessing necessary  
 305 for Deformable Diversity in 3D. We will continue with de-  
 306 scribing the matching process of a single mini template on  
 307 a full shape. Finally we will describe the extraction of mul-  
 308 tiple correspondences using this framework.

#### 309 3D Deformable Diversity Formulation

310 The nature of 3D data gives rise to unique problems  
 311 which do not occur in the 2D scenario. Data is distributed in  
 312 space both sparsely and with varying densities - the amount  
 313 of data points occupying a given volume can vary drasti-  
 314 cally.

315 A second problem arises from the absence of a regu-  
 316 lar grid. These problems require different definitions for

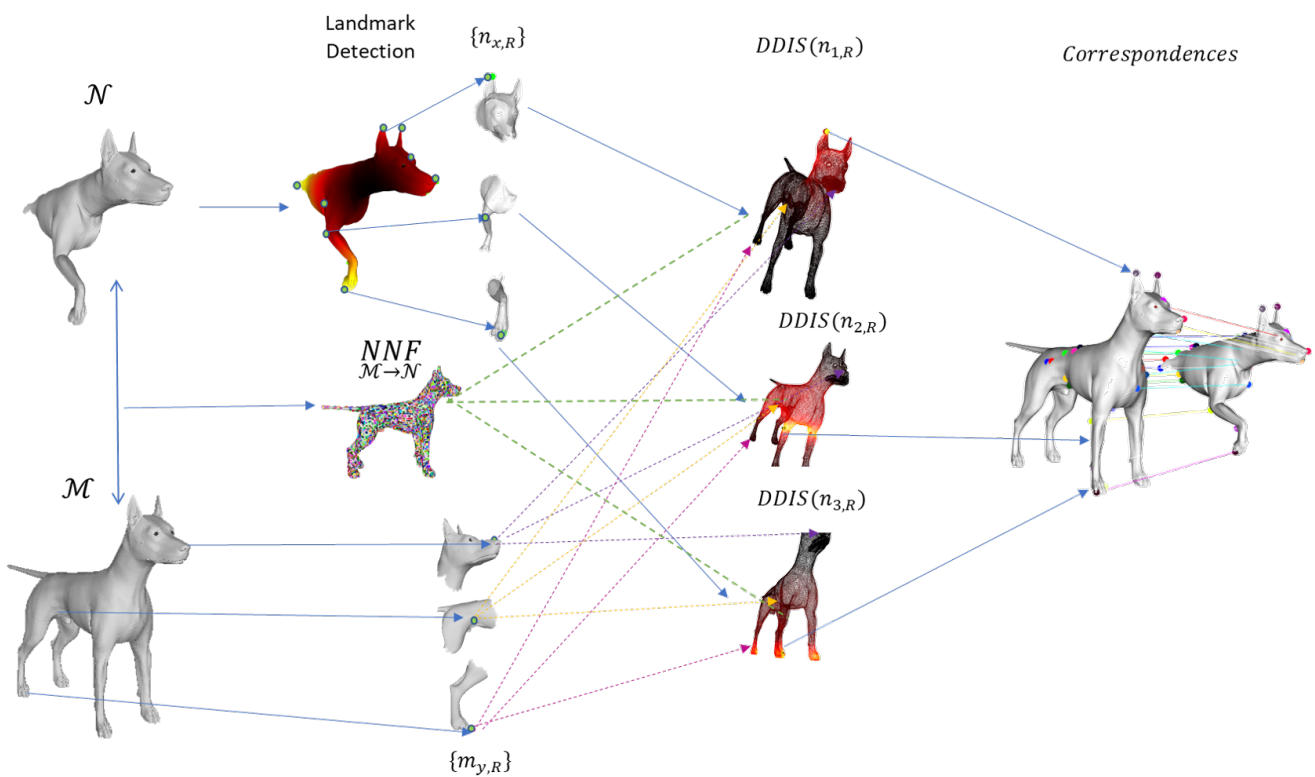
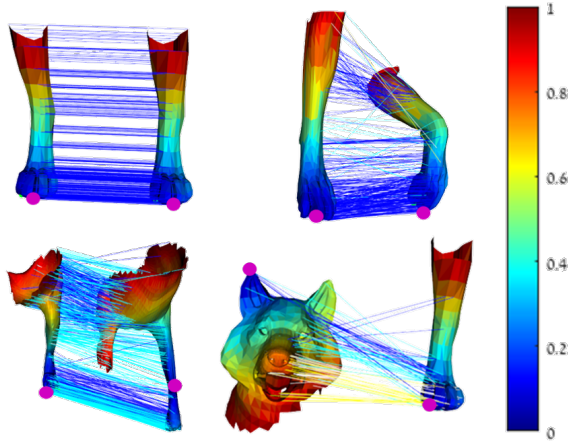


Figure 1. High level illustration of the DDIS Partial Correspondence pipe.



367  
368  
369  
370  
371  
372  
373  
374  
375  
376  
377

Figure 2. Illustration of Diversity Similarity between different shapes. Geodesic Distances are color coded by the jet scheme. You can notice that on identical pieces, and even on deformed matching pieces there are multiple diverse matches, most of which are colored in blue to indicated very similar distances from the source point, whereas on different pieces most lines map to very few points and a lot of yellow lines (high deformation) exist

key components to the 2D deformable diversity formulation. For this work we chose the image patch to be replaced

by a neighborhood which is required to calculate a selected shape descriptor, usually a small sphere in euclidean space or a surface patch in a small environment with a radius  $r_F$ . The search window of a template is replaced by a bigger environment around a chosen point, one which encompasses the entire desired part ,with a radius denoted by  $R$ . The pixel grid distance is replaced by either a euclidean distance  $d_{Euc}(x^l, y^l)$ (in the case of point cloud) or geodesic distance  $d_{Geo}(x^l, y^l)$ (for surface meshes). Given these DDIS between shape parts  $\mathcal{M}_{x,R}$  and  $\mathcal{N}_{y,R}$  can be naively formulated as:

$$DDIS = c \cdot \sum_{m_j \in \mathcal{M}_{x,R}} \frac{\exp(1 - \kappa(NN^S(m_j, \mathcal{N}_{y,R})))}{1 + r_j} \quad (4)$$

where  $\mathcal{M}_{x,R}$  and  $\mathcal{N}_{y,R}$  are the shape parts in a radius  $R$  surrounding the points  $m_x$  and  $n_y$  respectively, and  $r_j = |d(m_j^l, m_x^l) - d(NN^S(m_j, \mathcal{N}_{y,R})^l, n_y^l)| / (\gamma \cdot R)$ , where  $\gamma$  is a tunable parameter and  $c = 1 / \min|\mathcal{N}_{y,R}|, |\mathcal{M}_{x,R}|$ .

However, we wouldn't like to penalize our similarity score in case of repeating patterns or symmetrical shapes which have both symmetries in the template search window. Intuitively and empirically the exponent is too harsh and indeed unnecessary as both deformity and diversity will attenuate the score in case of multiple nearest neighbors. On the other hand, we wouldn't want to reward far correspondences at all. **explain why – can we see it visually**

432 on the same example? no visual example yet, as the partition  
 433 into smaller templates mitigates some of the problems  
 434 of the old formulation it seems, though the new one has  
 435 still given an extra 2 percent of accurate matches even in  
 436 the mini template setting To account for this the following  
 437 formulation has been found to work better: given a point  
 438  $n_i \in \mathcal{N}_{y,R}$  has a set of points  $\mathcal{M}_{n_i} = \{m_j \in \mathcal{M}_{j,R} : NNS(m_j, \mathcal{N}_{y,R}) = n_i\}$  for which it is the nearest neighbor,  
 439 we define  $m'_i = \operatorname{argmin}_{m_j \in \mathcal{M}_{n_i}}(r_j)$  and  $r'_i$  the minimal distortion distance our corrected formula becomes

$$DDIS(\mathcal{N}_{y,R}, \mathcal{M}_{x,R}, \gamma) = \sum_{m'_i} \frac{1}{1 + r'_i} \quad (5)$$

This equation still promotes both diversity and low deformations, but is less biased towards unsymmetrical surfaces.

#### Algorithm 1 3DIS Correspondence

```

procedure DDIS MATCH( $\mathcal{M}, n_y, \mathcal{N}, R_{thresh}, NNF_{\mathcal{M} \rightarrow \mathcal{N}}$ )
  Returns the location of the  $n_i \in \mathcal{N}$  in  $\mathcal{M}$ 
   $\mathcal{N}_{y,R} \leftarrow \{N_i \in \mathcal{N} : d_{Geo}(n_i, n_x) < R_{thresh}\}$ 
   $Similarity_{max} \leftarrow 0$ 
  for  $m_x \in \mathcal{M}$  do           ▷ DDIS calculation Loop
     $\mathcal{M}_{x,R} \leftarrow \{m_j \in \mathcal{M} : d_{Geo}(m_x, m_j) < 1.05 \cdot R_{thresh}\}$ 
     $Similarity[x] \leftarrow DDIS(\mathcal{M}_{x,R}, \mathcal{N}_{y,R})$ 
    if  $Similarity[x] > Similarity_{max}$  then
       $Similarity_{max} \leftarrow Similarity[x]$ 
       $m_y^* \leftarrow m_x$ 
    end if
  end for
  return  $m_y^*$ 
end procedure

```

### 3.1. DDIS Template Matching

**Goal of the algorithm** In this section we go over the flow of template matching of 3D shapes using DDIS, the solution of which constitutes the core of our partial shape matching. Given a template  $\mathcal{N}_{y,R}$  with a reference point  $n_y$  as its center and a maximal distance  $R$ , we aim to find on and object  $\mathcal{M}$  which has a deformed version of it, the corresponding surface piece  $\mathcal{M}_{y^*,R}$  and its center  $m_{y^*}$ . The solution is obtained by finding the point on  $\mathcal{M}$  whose surrounding surface maximizes the above mentioned DDIS measure. **key ideas**

**Overview** We'll first give an overview, and then give an extended description of each of each stage.

We start by calculating the normals for  $\mathcal{M}$  and  $\mathcal{N}$ . We than calculate local patch descriptors for each patch of some neighborhood around the points in each mesh(For our purpose FPFH seemed to work the best of our tested descriptors). Having calculated these descriptors we calculate a

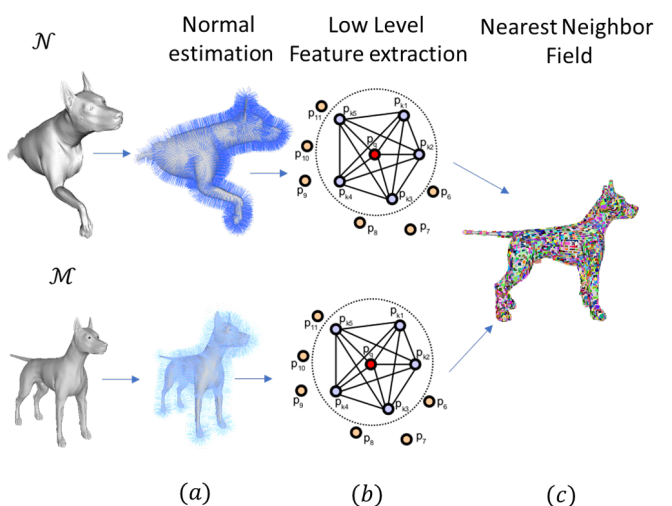


Figure 3. Nearest Neighbor Field calculation.

nearest neighbor field by finding for each patch in  $\mathcal{M}$  it's Nearest Neighbor in  $\mathcal{N}$ . We now find the distance of every point  $n \in \mathcal{N}$  to the desired point  $n_y$  for a desired neighborhood  $R$ . We now go over every point  $m_x \in \mathcal{M}$ . For each we extract the surface  $\mathcal{M}_{x,R}$  in an  $R$  neighborhood around it. We take notice that while the above stages are done here in the context of template matching for one template, when matching multiple templates all of the above calculations have to be done only once between the shapes, with the exception of geodesic distance field extraction for the template itself.

Now we calculate our DDIS similarity measure of this surface with  $\mathcal{N}_{x,R}$  which has  $n_y$  as it's center. Having done that for every location, the point  $m_{y^*}$  which gets the maximal DDIS Score is deemed the corresponding point to  $n_y$ .

**Point Normal Estimation** There are various schemes for the estimation of point normals given a triangulated mesh surface. We have picked the one which is available in the standard PCL. Given a vertex  $p_i$  on a triangulated mesh  $\mathcal{X}$  and it's associated polygons  $\{A_j\}_{j=1}^k$  and their normals  $N_{A_j}$  the point normal  $N_i = \sum_{j=1}^k |A_j| \cdot N_{A_j}$

**Local Patch Size choice** DDIS as defined by [] uses patch descriptors as low level features for their similarity measure. While a patch in an image can by defined by the images grid no such grid exists on 3D point clouds and meshes, where density of data points can vary. Thus a patch has to be defined by some geometric measure. While the more robust way to define it would be using geodesic distance, since we are talking a small environment around a point on the mesh we have found that for practical purposes a patch in a defined euclidean radius around a point serves well enough. We pick this radius in the following way: given the full surface mesh  $\mathcal{M}$  we define a characteristic length  $D_{\mathcal{M}} = \sqrt{\text{Area}(\mathcal{M})}$ , and tune a parameter  $\alpha$  to ob-

540 tain  $r_F = \frac{\alpha}{100} * D_{\mathcal{M}}$

541 **Local Patch Descriptor** A lot of local shape descriptors have been used successfully in 3D shape analysis.  
 542 We have tested the following descriptors which are included in the Point Cloud Library: ROPS[?, Theorem  
 543 2] PFH[] SHOT[], HKS[], SIHKS[], ROPS[] and FPFH[]. Out of these 4 FPFH has achieved the best performance,  
 544 and thus the descriptor for the local patch has been chosen to be FPFH. **Nearest Neighbor Field** As an intermediate stage towards the calculation of Deformable Diversity Similarity measure, the calculation of the nearest neighbor field(will be abbreviated as NNF) needs to be calculated. Thus for every patch  $m \in \mathcal{M}$  we have to find the patch on the template  $n \in \mathcal{N}$  which resembles it the most. For  $F_{PFH}$ ,  $NN^S(m_j, \mathcal{N})$  is defined  
 545  $NN^S(m_j, \mathcal{N}) \equiv \underset{i}{\operatorname{argmin}} \chi^2(F_{PFH}(m_j], F_{PFH}(n_i))$   
 546 and the Nearest Neighbor Field is the set of all these correspondences.  
 547

548 **DDIS calculation** For every point in  $m_x \in \mathcal{M}$  we then extract a surface part  $\mathcal{M}_{x,R}$  with a radius  $R$  around it and calculate deformable diversity around it. The point which maximizes DDIS gives us a correspondence  $(n_y, m_y*)$ . Since as we will show in the results section, imperfections in the isometry assumption lead to considerable localization errors, we move to a multiple template matching framework using DDIS, as will be described in the next section.

### 549 3.2. DDIS Sparse Correspondences

550 A key takeaway from experimenting with DDIS as a template matching algorithm for partial matching has been that isometry does not hold, at least not globally. It does however, hold pretty well locally, especially at extremities. To this end we devise multiple template framework for Partial correspondences of deformable shape. We first obtain the landmarks  $F = \{f\}_i$  as described in[ ]. We then choose a partiality radius  $R = \gamma \cdot R$  and extract surface parts  $\mathcal{N}_{i,R}$  around each extremity point. Finally for each point we calculate DDIS to get it's correspondence.

551 **Landmark Extraction** We follow the work of [Sagi Katz Ayellet Tal] to obtain interesting landmark points. Given a shape the work employs the following framework to extract it's extremities. A point is detected as an extremity if it fulfills 2 conditions: - it's sum of geodesic distances is a local extrema, formally, for  $v \in S$ , where  $S$  is a surface mesh, we define the set of points with a direct edge to it as  $N_v$ , the point is a critical point if :

$$\sum_{v_i \in S} d_{geo}(v, v_i) > \sum_{v_i \in S} d_{geo}(v_n, v_i), \forall v_n \in N_v \quad (6)$$

552 An additional requirement for it to be an extremities is for it to lie on the convex hull of the shape's MDS. In this work we have dropped the last condition, but chose  $N_{v*}$  - a neighborhood of  $0.03 \cdot \sqrt{\text{Area}(S)}$ .

---

### 553 Algorithm 2 3DIS Sparse Correspondences

```

554 procedure DDIS CORRESPONDENCE( $\mathcal{M}, \mathcal{N}, \alpha, \beta, \gamma$ )  $\triangleright$ 
555   Returns point correspondence for critical points on  $\mathcal{N}$ 
556    $r_F \leftarrow \alpha/100 \cdot \sqrt{\text{Area}(\mathcal{M})}$ 
557    $R_{thresh} \leftarrow \beta/100 \cdot \sqrt{\text{Area}(\mathcal{M})}$ 
558    $N_{\mathcal{M}} \leftarrow \text{ComputeNormals}(\mathcal{M})$ 
559    $N_{\mathcal{N}} \leftarrow \text{ComputeNormals}(\mathcal{N})$ 
560    $F_{\mathcal{M}} \leftarrow F_{PFH}(\mathcal{M}, N_{\mathcal{M}}, r_F)$ 
561    $F_{\mathcal{N}} \leftarrow F_{PFH}(\mathcal{N}, N_{\mathcal{N}}, r_F)$ 
562    $NNF_{\mathcal{M} \rightarrow \mathcal{N}} \leftarrow ANN(F_{\mathcal{M}}, F_{\mathcal{N}})$ 
563    $\mathcal{N}_c = \{n : \sum_{n_i \in \mathcal{N}} d_{geo}(n, n_i) > 0.03 \cdot \sqrt{\text{Area}(\mathcal{M})}\}$ 
564    $\forall n_N : d_{geo}(n, n_N) <$ 
565    $\text{for } n_y \in \mathcal{N}_c \text{ do} \quad \triangleright \text{DDIS calculation Loop}$ 
566      $m_{c*} \leftarrow DDIS\_Correspondence(\mathcal{M}, n_y, \mathcal{N}, \alpha, \beta, \gamma)$ 
567    $\text{end for}$ 
568   return  $\mathcal{M}_c \times \mathcal{N}_c = \{m_{c*}, n_c\}$ 
569 end procedure

```

---

570 **Landmark Template Matching** For this end, we create a template for each landmark point - we collect all surface point in a geodesic neighborhood around it of  $\beta \cdot \sqrt{\text{area}(\mathcal{M})}$  where for this case a good  $\beta$  (0.2, 0.5) where larger beta prevents global scale error, such as a cats paw being mapped to a hind paw, while smaller beta promotes tighter localization on the part itself. This can be seen in Figure[] While it might seem natural to calculate a different nearest neighbor field for each landmark template it has been empirically found that using the global nearest neighbor field gives much better results. This is probably due to the fact that the nearest neighbor field encodes global information when obtained this way and eliminates local distractors. Each landmark template is compared to all surface parts of a similar  $R$  on  $\mathcal{M}$  to obtain final point correspondences.

### 571 3.3. Cascaded Multi-Scale DDIS

572 The observation of the effects of the choice of  $\beta$  and the trade-off between finer localization and avoidance of global errors naturally leads to the adoption of a multi scale framework. We calculate *DDIS* score for multiple *beta* values, and use the location obtained with a large beta to select a narrow environment in which we look for the maximum of DDIS with a smaller value *beta*, thus using the larger scale to get a rough global location, and the smaller scale to fit it into a more exact location. While this might be done at multiple custom scales we have found that the triplet  $\beta, 2 \cdot \text{beta}/3\beta/3$  works well.

## 573 4. Experiments and results

574 In this section we will briefly go over the experiments performed and their results. We'll introduce the datasets,

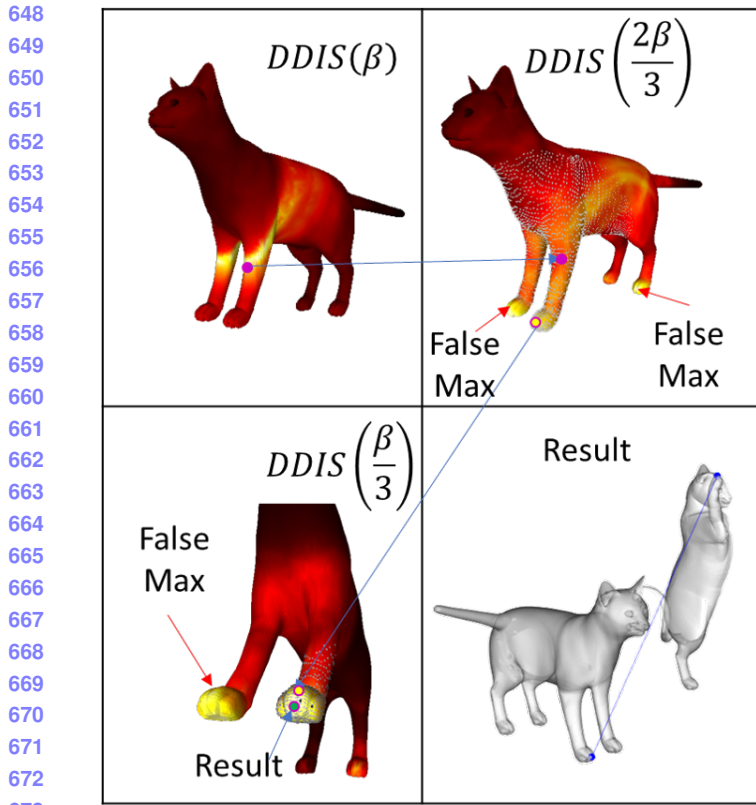


Figure 4. Illustration of the multi scale framework. Gray point are the area chosen by the previous scale to be valid. It can be seen that Wrong maxima in lower scales are ignored due to this process

detail our experiments and their results

## 4.1. Datasets

In this section we will briefly go over the available Datasets

### 4.1.1 SHREC 2016

The SHREC partial matching dataset consists of 8 base, neutral pose models: cat, centaur, dog, horse, wolf, and 3 humans 2 males, and 1 female. Each basic model has corresponding deformed partial shapes obtained either by cutting the shape with a plane or by adding holes on a deformed shape. The set has been divided into train and test sets. The train set is composed of 15 cuts for each base models totaling 120 models, and 10 holed shpaes for each model for which ground truth point to polygon correspondences has been provided in barycentric coordinates. The test set is composed of additional 200 cuts and 200 holed shapes.

## 4.2. Error Metrics

The output of partial matching algorithms (as defined in [8]) are sub-vertex point-to-point correspondences between partial shapes. For all experiments we use the standard practice of not penalizing symmetric solutions. Quality is measured according to the Princeton benchmark protocol [10]. For a pair of points  $(x, y) \in \mathcal{N} \times \mathcal{M}$  between the full object  $\mathcal{M}$  and the partial shape  $\mathcal{N}$  produced by an algorithm, where  $(x, y^*)$  is the ground truth correspondence the inaccuracy is measured by

$$\varepsilon(x) = \frac{d_{\mathcal{M}}(y, y^*)}{\sqrt{\text{area}(\mathcal{M})}} \quad (7)$$

where  $d_{\mathcal{M}}(y, y^*)$  is the geodesic distance on  $\mathcal{M}$ , and has units of normalized length on  $\mathcal{M}$ . For dense correspondences over a dataset,  $\varepsilon(x)$  is averaged over all matching instances.

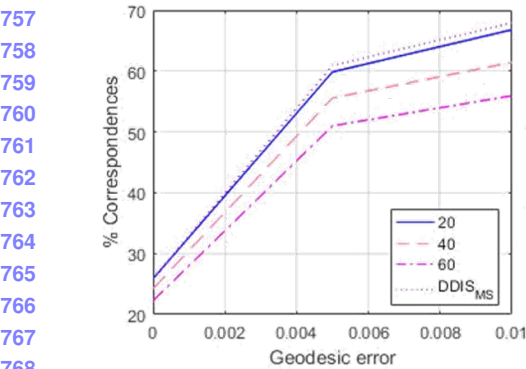
### 4.2.1 Central Points Localization

In this experiment we have chosen for each Template mesh the center point  $c_T$  and tried to match it to a point on the object using DDIS. Experiments have been done using FPFH, PFH and SHOT as patch descriptors with patch radiiuses of  $[2, 3, 4, 5]$ , the results of the opimal parameter for each descriptor are illustrated in fig. and visualizations of similarity maps of cuts are provided in fig. . It can be seen that good localization is obtained for points on a smooth surface, under high partiality conditions and strong deformations. Bad matches occur when a matched point resides on a heavily deformed patch, and when salient anchor points are deformed or cut. Analysis of these results shows a drift in localization occurs when salient features are divided by strong unisometric deformations which serve as the motivation for the multiple template matching framework.

## 4.3. Sparse Correspondences on the SHREC16 Test set

In this experiment we have tested the performance of DDIS in producing sparse correspondences on the SHREC16 Partial Matching of Deformable Shapes competition. We had tuned our parameters on the SHREC16 training dataset using only the cuts part of it. The best results had been produced using FPFH with  $r_F = 0.04\sqrt{\text{Area}(\mathcal{M})}$ , and a piece size radius  $R_{thresh} = 0.3\sqrt{\text{Area}(\mathcal{M})}$ . For Geodesic distances we have found the fast marching algorithm to work the fastest, while giving the lowest error w.r.t. to exact geodesics. For a 10,000 vertices mesh it takes 60s to produce a full distance matrix, Though it should be noted this algorithm has a more efficient GPU implementation. FPFH and Nearest Neighbor field takes 2 s' and similarity between 2 pieces of 10000 vertices each takes 25s on

756



757

758  
759  
760  
761  
762  
763  
764  
765  
766  
767

Figure 5. Effect of the  $\beta$  parameter on the results: it can be seen that a smaller beta promotes better localization in a small neighborhood, while higher values of  $\beta$  lead to more local errors but are more robust to global errors. It can be seen that the multi-scale cascade achieves better results both locally and globally.

768

769

770

771

772

773

774

775

776

777

778

779

780

781

782

783

784

785

786

787

788

789

790

791

792

793

794

795

796

797

798

799

800

801

802

803

804

805

806

807

808

809

810

811

812

813

814

815

816

817

818

819

820

821

822

823

824

825

826

827

828

829

830

831

832

833

834

835

836

837

838

839

840

841

842

843

844

845

846

847

848

849

850

851

852

853

854

855

856

857

858

859

860

861

862

863

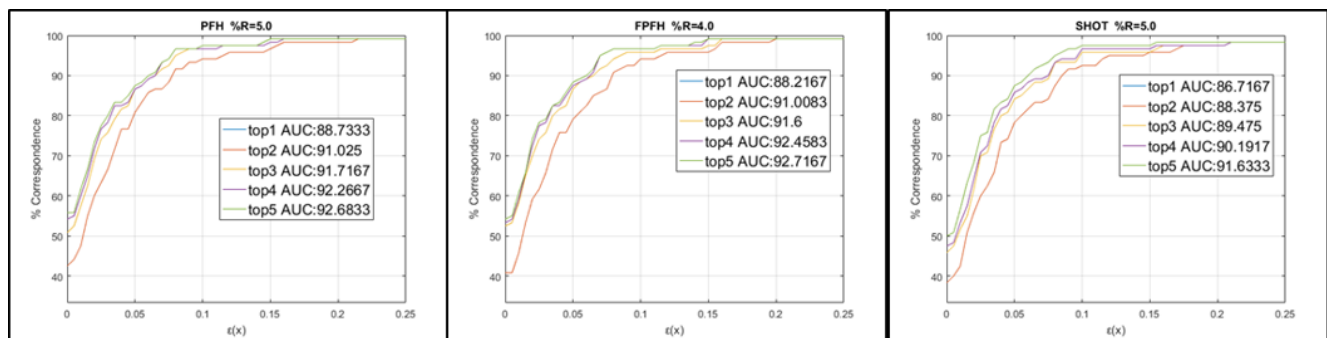


Figure 6. Comparison between descriptors: we show curves for the minimal distance of the top results. a noticeable addition occurs when adding the 2nd best match

average, running on a single thread of i7-2700k. Unlike optimization based algorithms this is highly parallelizable. We achieve results comparable to the state of the art [12] quality wise, even though sparser in nature on both the Cuts and the Holes datasets, Where a particularly impressive result is reported on the Holes dataset. A further look reveals even more reliable results can be obtained taking only the extremity points not lying on the mesh longest boundary, but they will be more sparse

	PFM	RF	IM	EN	GT	DIS	DISnoBound
cuts	dense	dense	61.3	87.8	51.0	27.9	14.5
holes	dense	dense	78.2	112.6	76.4	77.3	52.11

Table 1. mean number of correspondence obtained by the algorithms in the SHREC 16 competition and our algorithm

## References

- [1] D. Aiger, N. J. Mitra, and D. Cohen-Or. 4pointss congruent sets for robust pairwise surface registration. *ACM Trans. Graph.*, 27(3):85:1–85:10, Aug. 2008. 2
- [2] N. Aigerman, R. Poranne, and Y. Lipman. Seamless surface mappings. *ACM Transactions on Graphics (TOG)*, 34(4):72, 2015. 2
- [3] M. Aubry, U. Schlickewei, and D. Cremers. The wave kernel signature: A quantum mechanical approach to shape analysis. In *Computer Vision Workshops (ICCV Workshops), 2011 IEEE International Conference on*, pages 1626–1633. IEEE, 2011. 2
- [4] A. M. Bronstein and M. M. Bronstein. Not only size matters: regularized partial matching of nonrigid shapes. In *Computer Vision and Pattern Recognition Workshops, 2008. CVPRW’08. IEEE Computer Society Conference on*, pages 1–6. IEEE, 2008. 1, 2
- [5] A.-M. Bronstein, M. M. Bronstein, A. M. Bruckstein, and R. Kimmel. Partial similarity of objects, or how to compare a centaur to a horse. *International Journal of Computer Vision*, 84(2):163, 2009. 2
- [6] A. M. Bronstein, M. M. Bronstein, and R. Kimmel. Generalized multidimensional scaling: a framework for isometry-invariant partial surface matching. *Proceedings of the National Academy of Sciences*, 103(5):1168–1172, 2006. 1, 2
- [7] M. M. Bronstein and I. Kokkinos. Scale-invariant heat kernel signatures for non-rigid shape recognition. In *Computer Vision and Pattern Recognition (CVPR), 2010 IEEE Conference on*, pages 1704–1711. IEEE, 2010. 2
- [8] L. Cosmo, E. Rodolà, M. Bronstein, A. Torsello, D. Cremers, and Y. Sahillioglu. Shrec16: Partial matching of deformable shapes. *Proc. 3DOR*, 2, 2016. 7

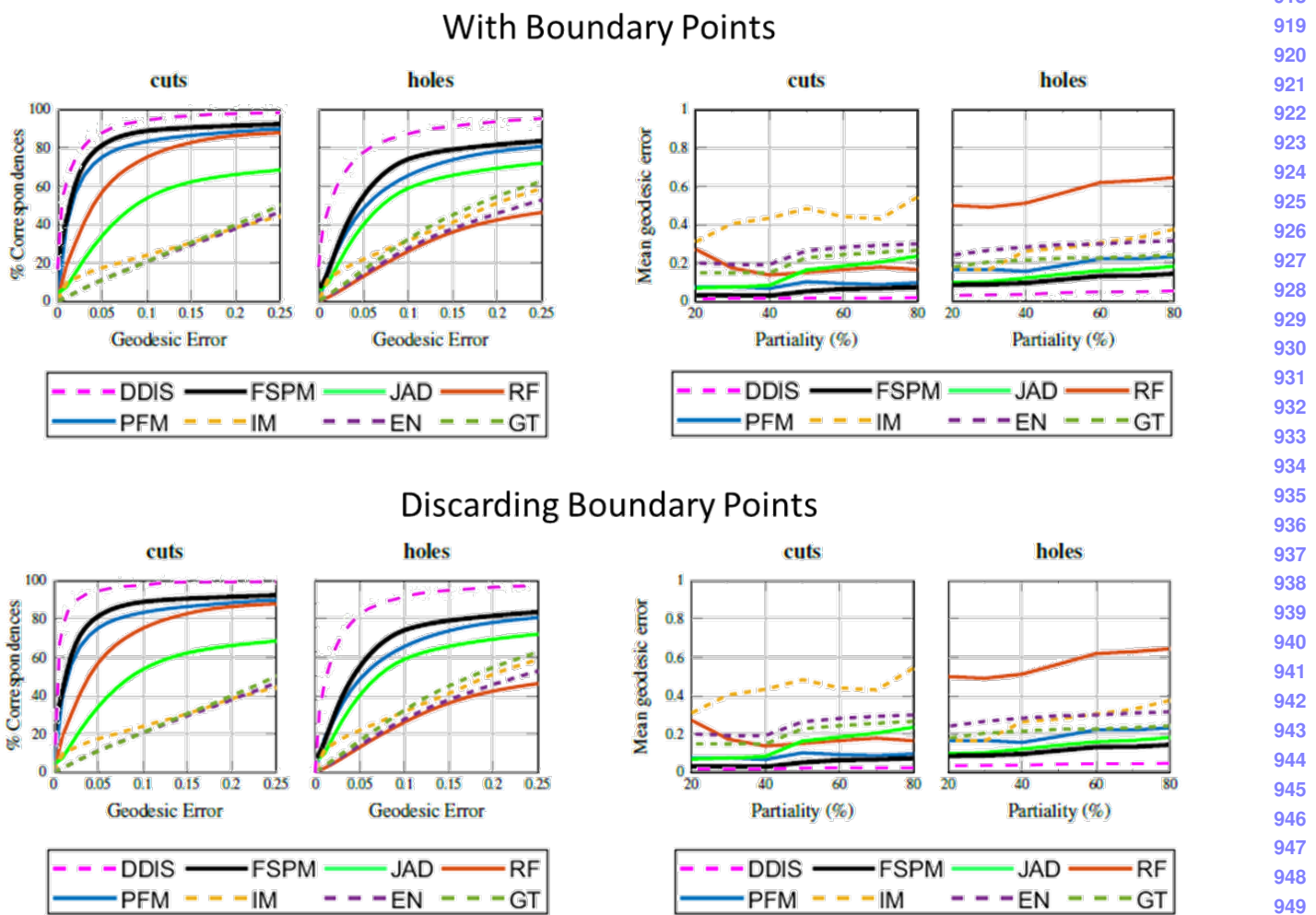


Figure 7. comparison with other state of the art algorithms - it can be seen that although sparse in nature, the correspondence obtained by DDIS are much more accurate than the other methods. A separate analysis has been done for correspondences which include boundary points, which tend to be more noisy, and internal points which are more sparse

- [9] T. Dekel, S. Oron, M. Rubinstein, S. Avidan, and W. T. Freeman. Best-buddies similarity for robust template matching. In *Proceedings of the IEEE Conference on Computer Vision and Pattern Recognition*, pages 2021–2029, 2015. 2
- [10] V. G. Kim, Y. Lipman, and T. Funkhouser. Blended intrinsic maps. In *ACM Transactions on Graphics (TOG)*, volume 30, page 79. ACM, 2011. 7
- [11] A. Kovnatsky, M. M. Bronstein, X. Bresson, and P. Vandergheynst. Functional correspondence by matrix completion. In *Proceedings of the IEEE conference on computer vision and pattern recognition*, pages 905–914, 2015. 2
- [12] O. Litany, E. Rodolà, A. M. Bronstein, and M. M. Bronstein. Fully spectral partial shape matching. In *Computer Graphics Forum*, volume 36, pages 247–258. Wiley Online Library, 2017. 1, 2, 8
- [13] H. Maron, N. Dym, I. Kezurer, S. Kovalsky, and Y. Lipman. Point registration via efficient convex relaxation. *ACM Transactions on Graphics (TOG)*, 35(4):73, 2016. 2

- [14] M. Ovsjanikov, M. Ben-Chen, J. Solomon, A. Butscher, and L. Guibas. Functional maps: A flexible representation of maps between shapes. *ACM Trans. Graph.*, 31(4):30:1–30:11, July 2012. 1, 2
- [15] J. Pokrass, A. M. Bronstein, and M. M. Bronstein. Partial shape matching without point-wise correspondence. *Numerical Mathematics: Theory, Methods and Applications*, 6(1):223–244, 2013. 2
- [16] J. Pokrass, A. M. Bronstein, M. M. Bronstein, P. Sprechmann, and G. Sapiro. Sparse modeling of intrinsic correspondences. In *Computer Graphics Forum*, volume 32, pages 459–468. Wiley Online Library, 2013. 2
- [17] E. Rodolà, L. Cosmo, M. M. Bronstein, A. Torsello, and D. Cremers. Partial functional correspondence. In *Computer Graphics Forum*, volume 36, pages 222–236. Wiley Online Library, 2017. 1, 2
- [18] E. Rodola, A. Torsello, T. Harada, Y. Kuniyoshi, and D. Cremers. Elastic net constraints for shape matching. In *Pro-*

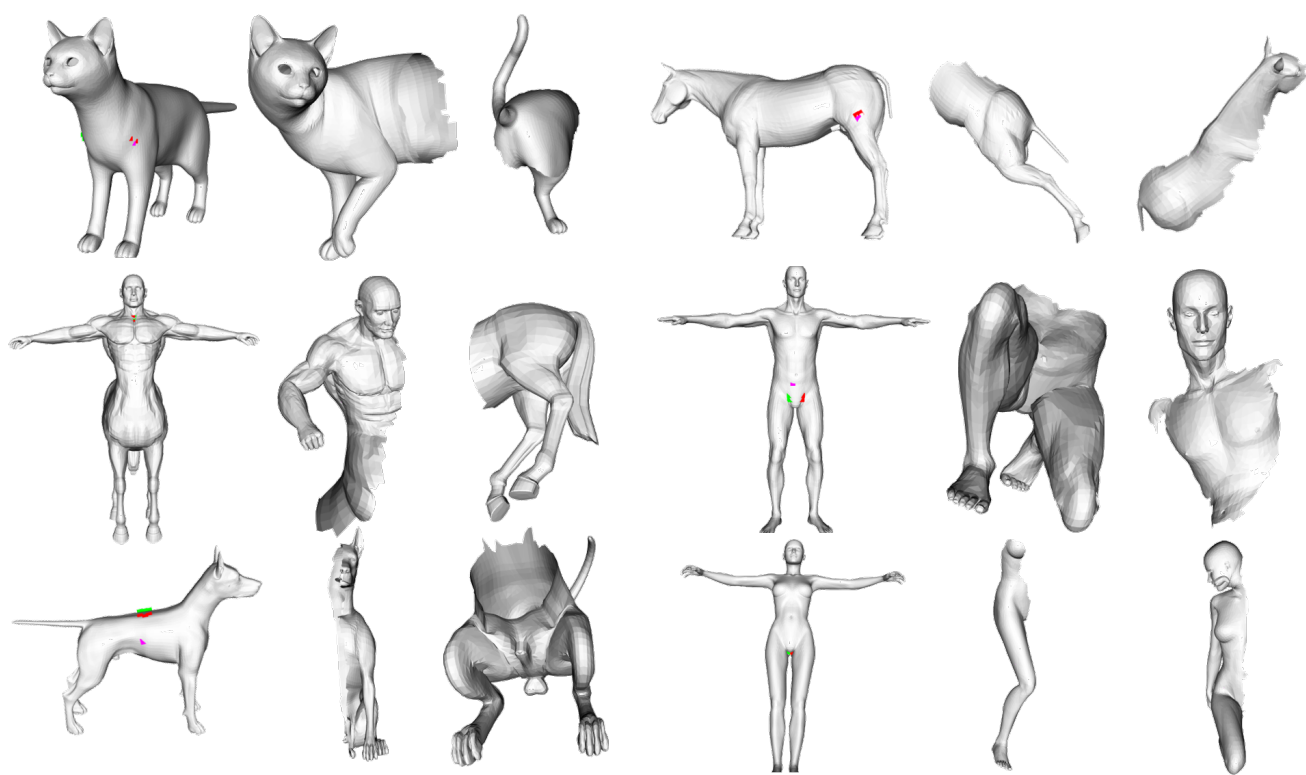


Figure 8. SHREC 16 cuts partial matching dataset.

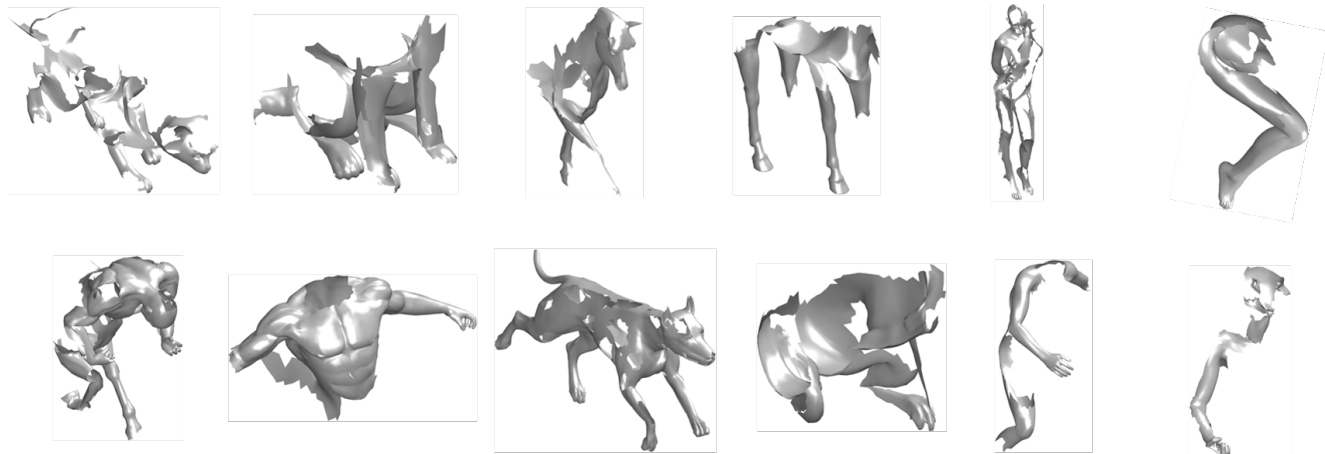


Figure 9. SHREC 16 holes partial matching dataset.

ceedings of the IEEE International Conference on Computer Vision, pages 1169–1176, 2013. 2

sion, 2008. ICARCV 2008. 10th International Conference on, pages 643–650. IEEE, 2008. 2

- [19] R. B. Rusu, N. Blodow, and M. Beetz. Fast point feature histograms (fpfh) for 3d registration. In *Robotics and Automation, 2009. ICRA'09. IEEE International Conference on*, pages 3212–3217. Citeseer, 2009. 2
- [20] R. B. Rusu, Z. C. Marton, N. Blodow, and M. Beetz. Learning informative point classes for the acquisition of object model maps. In *Control, Automation, Robotics and Vi-*

- sion, 2008. ICARCV 2008. 10th International Conference on*, pages 643–650. IEEE, 2008. 2
- [21] R. B. Rusu, Z. C. Marton, N. Blodow, M. Dolha, and M. Beetz. Towards 3d point cloud based object maps for household environments. *Robotics and Autonomous Systems*, 56(11):927–941, 2008. 2
- [22] Y. Sahillioğlu and Y. Yemez. Scale normalization for isometric shape matching. In *Computer Graphics Forum*, volume 31, pages 2233–2240. Wiley Online Library, 2012. 2

- 1080 [23] Y. Sahillioğlu and Y. Yemez. Multiple shape correspondence  
1081 by dynamic programming. In *Computer Graphics Forum*,  
1082 volume 33, pages 121–130. Wiley Online Library, 2014. 2 1134  
1083 [24] J. Solomon, G. Peyré, V. G. Kim, and S. Sra. Entropic metric  
1084 alignment for correspondence problems. *ACM Transactions  
1085 on Graphics (TOG)*, 35(4):72, 2016. 2 1135  
1086 [25] I. Talmi, R. Mechrez, and L. Zelnik-Manor. Template matching  
1087 with deformable diversity similarity. In *Proc. of IEEE  
1088 Conf. on Computer Vision and Pattern Recognition*, pages  
1089 1311–1319, 2017. 1, 3 1136  
1090 [26] A. Torsello. A game-theoretic approach to deformable shape  
1091 matching. In *Proceedings of the 2012 IEEE Conference on  
1092 Computer Vision and Pattern Recognition (CVPR)*, CVPR  
1093 ’12, pages 182–189, Washington, DC, USA, 2012. IEEE  
1094 Computer Society. 1, 2 1137  
1095 [27] M. Vestner, Z. Lähner, A. Boyarski, O. Litany, R. Slossberg,  
1096 T. Remez, E. Rodola, A. Bronstein, M. Bronstein, R. Kimmel,  
1097 et al. Efficient deformable shape correspondence via  
1098 kernel matching. In *3D Vision (3DV), 2017 International  
1099 Conference on*, pages 517–526. IEEE, 2017. 1, 2 1138  
1100 [28] M. Vestner, R. Litman, E. Rodolà, A. M. Bronstein, and  
1101 D. Cremers. Product manifold filter: Non-rigid shape corre-  
1102 spondence via kernel density estimation in the product space.  
In *CVPR*, pages 6681–6690, 2017. 2 1139  
1103  
1104 

## References

  
1105 [1] D. Aiger, N. J. Mitra, and D. Cohen-Or. 4pointss congruent  
1106 sets for robust pairwise surface registration. *ACM Trans.  
1107 Graph.*, 27(3):85:1–85:10, Aug. 2008. 2 1140  
1108 [2] N. Aigerman, R. Poranne, and Y. Lipman. Seamless surface  
1109 mappings. *ACM Transactions on Graphics (TOG)*, 34(4):72,  
1110 2015. 2 1141  
1111 [3] M. Aubry, U. Schlickewei, and D. Cremers. The wave kernel  
1112 signature: A quantum mechanical approach to shape analy-  
1113 sis. In *Computer Vision Workshops (ICCV Workshops), 2011  
1114 IEEE International Conference on*, pages 1626–1633. IEEE,  
1115 2011. 2 1142  
1116 [4] A. M. Bronstein and M. M. Bronstein. Not only size mat-  
1117 ters: regularized partial matching of nonrigid shapes. In  
1118 *Computer Vision and Pattern Recognition Workshops, 2008.  
1119 CVPRW’08. IEEE Computer Society Conference on*, pages  
1–6. IEEE, 2008. 1, 2 1143  
1120 [5] A. M. Bronstein, M. M. Bronstein, A. M. Bruckstein, and  
1121 R. Kimmel. Partial similarity of objects, or how to compare a  
1122 centaur to a horse. *International Journal of Computer Vision*,  
1123 84(2):163, 2009. 2 1144  
1124 [6] A. M. Bronstein, M. M. Bronstein, and R. Kimmel. General-  
1125 ized multidimensional scaling: a framework for isometry-  
1126 invariant partial surface matching. *Proceedings of the Na-  
1127 tional Academy of Sciences*, 103(5):1168–1172, 2006. 1, 2 1145  
1128 [7] M. M. Bronstein and I. Kokkinos. Scale-invariant heat ker-  
1129 nel signatures for non-rigid shape recognition. In *Computer  
1130 Vision and Pattern Recognition (CVPR), 2010 IEEE Confer-  
1131 ence on*, pages 1704–1711. IEEE, 2010. 2 1146  
1132 [8] L. Cosmo, E. Rodolà, M. Bronstein, A. Torsello, D. Cremers,  
1133 and Y. Sahillioglu. Shrec16: Partial matching of deformable  
shapes. *Proc. 3DOR*, 2, 2016. 7 1147  
1134 [9] T. Dekel, S. Oron, M. Rubinstein, S. Avidan, and W. T. Free-  
1135 man. Best-buddies similarity for robust template matching.  
In *Proceedings of the IEEE Conference on Computer Vision  
1136 and Pattern Recognition*, pages 2021–2029, 2015. 2 1148  
1137 [10] V. G. Kim, Y. Lipman, and T. Funkhouser. Blended intrinsic  
1138 maps. In *ACM Transactions on Graphics (TOG)*, volume 30,  
1139 page 79. ACM, 2011. 7 1149  
1140 [11] A. Kovnatsky, M. M. Bronstein, X. Bresson, and P. Van-  
1141 derghenst. Functional correspondence by matrix comple-  
1142 tion. In *Proceedings of the IEEE conference on computer  
1143 vision and pattern recognition*, pages 905–914, 2015. 2 1144  
1143 [12] O. Litany, E. Rodolà, A. M. Bronstein, and M. M. Bronstein.  
1144 Fully spectral partial shape matching. In *Computer Graphics  
1145 Forum*, volume 36, pages 247–258. Wiley Online Library,  
1146 2017. 1, 2, 8 1147  
1147 [13] H. Maron, N. Dym, I. Kezurer, S. Kovalsky, and Y. Lip-  
1148 man. Point registration via efficient convex relaxation. *ACM  
1149 Transactions on Graphics (TOG)*, 35(4):73, 2016. 2 1150  
1149 [14] M. Ovsjanikov, M. Ben-Chen, J. Solomon, A. Butscher, and  
1150 L. Guibas. Functional maps: A flexible representation of  
1151 maps between shapes. *ACM Trans. Graph.*, 31(4):30:1–  
1152 30:11, July 2012. 1, 2 1153  
1153 [15] J. Pokrass, A. M. Bronstein, and M. M. Bronstein. Partial  
1154 shape matching without point-wise correspondence. *Nu-  
1155 matical Mathematics: Theory, Methods and Applications*,  
1156 6(1):223–244, 2013. 2 1157  
1157 [16] J. Pokrass, A. M. Bronstein, M. M. Bronstein, P. Sprech-  
1158 mann, and G. Sapiro. Sparse modeling of intrinsic cor-  
1159 respondences. In *Computer Graphics Forum*, volume 32,  
1160 pages 459–468. Wiley Online Library, 2013. 2 1161  
1161 [17] E. Rodolà, L. Cosmo, M. M. Bronstein, A. Torsello, and  
1162 D. Cremers. Partial functional correspondence. In *Computer  
1163 Graphics Forum*, volume 36, pages 222–236. Wiley Online  
1164 Library, 2017. 1, 2 1165  
1165 [18] E. Rodola, A. Torsello, T. Harada, Y. Kuniyoshi, and D. Cre-  
1166 mers. Elastic net constraints for shape matching. In *Pro-  
1167 ceedings of the IEEE International Conference on Computer  
1168 Vision*, pages 1169–1176, 2013. 2 1169  
1169 [19] R. B. Rusu, N. Blodow, and M. Beetz. Fast point feature  
1170 histograms (fpfh) for 3d registration. In *Robotics and Au-  
1171 tonomation, 2009. ICRA’09. IEEE International Conference  
1172 on*, pages 3212–3217. Citeseer, 2009. 2 1173  
1173 [20] R. B. Rusu, Z. C. Marton, N. Blodow, and M. Beetz. Learn-  
1174 ing informative point classes for the acquisition of object  
1175 model maps. In *Control, Automation, Robotics and Vi-  
1176 sion, 2008. ICARCV 2008. 10th International Conference  
1177 on*, pages 643–650. IEEE, 2008. 2 1178  
1178 [21] R. B. Rusu, Z. C. Marton, N. Blodow, M. Dolha, and  
1179 M. Beetz. Towards 3d point cloud based object maps for  
1180 household environments. *Robotics and Autonomous Sys-  
1181 tems*, 56(11):927–941, 2008. 2 1182  
1182 [22] Y. Sahillioğlu and Y. Yemez. Scale normalization for iso-  
1183 metric shape matching. In *Computer Graphics Forum*, vol-  
1184 umne 31, pages 2233–2240. Wiley Online Library, 2012. 2 1185  
1185 [23] Y. Sahillioğlu and Y. Yemez. Multiple shape correspond-  
1186 ence by dynamic programming. In *Computer Graphics Forum*,  
1187 volume 33, pages 121–130. Wiley Online Library, 2014. 2 1188

- 1188 [24] J. Solomon, G. Peyré, V. G. Kim, and S. Sra. Entropic metric  
1189 alignment for correspondence problems. *ACM Transactions  
1190 on Graphics (TOG)*, 35(4):72, 2016. 2  
1191 [25] I. Talmi, R. Mechrez, and L. Zelnik-Manor. Template match-  
1192 ing with deformable diversity similarity. In *Proc. of IEEE  
1193 Conf. on Computer Vision and Pattern Recognition*, pages  
1194 1311–1319, 2017. 1, 3  
1195 [26] A. Torsello. A game-theoretic approach to deformable shape  
1196 matching. In *Proceedings of the 2012 IEEE Conference on  
1197 Computer Vision and Pattern Recognition (CVPR)*, CVPR  
1198 ’12, pages 182–189, Washington, DC, USA, 2012. IEEE  
1199 Computer Society. 1, 2  
1200 [27] M. Vestner, Z. Lähner, A. Boyarski, O. Litany, R. Slossberg,  
1201 T. Remez, E. Rodola, A. Bronstein, M. Bronstein, R. Kim-  
1202 mel, et al. Efficient deformable shape correspondence via  
1203 kernel matching. In *3D Vision (3DV), 2017 International  
1204 Conference on*, pages 517–526. IEEE, 2017. 1, 2  
1205 [28] M. Vestner, R. Litman, E. Rodolà, A. M. Bronstein, and  
1206 D. Cremers. Product manifold filter: Non-rigid shape corre-  
1207 spondence via kernel density estimation in the product space.  
1208 In *CVPR*, pages 6681–6690, 2017. 2  
1209  
1210  
1211  
1212  
1213  
1214  
1215  
1216  
1217  
1218  
1219  
1220  
1221  
1222  
1223  
1224  
1225  
1226  
1227  
1228  
1229  
1230  
1231  
1232  
1233  
1234  
1235  
1236  
1237  
1238  
1239  
1240  
1241

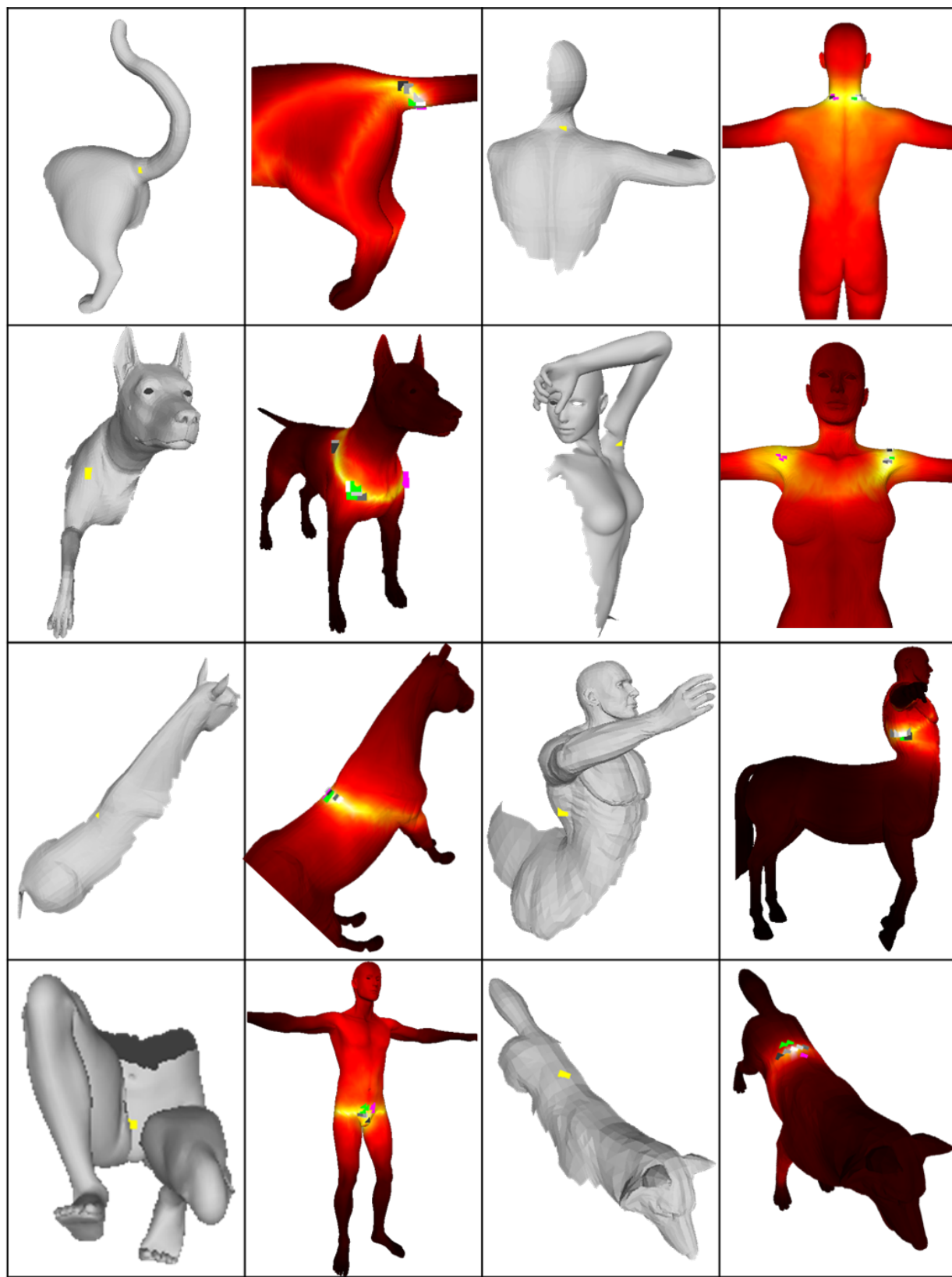
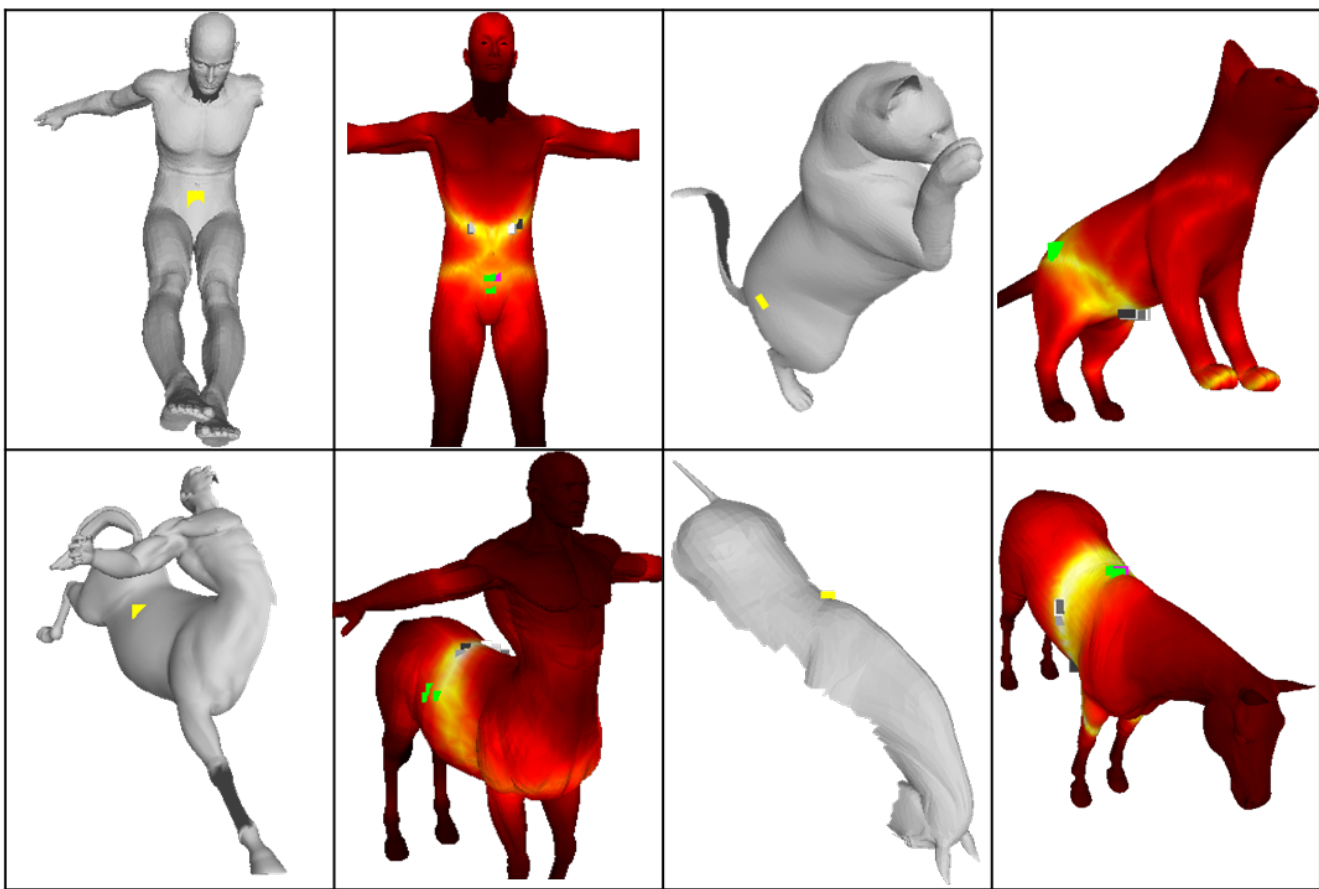
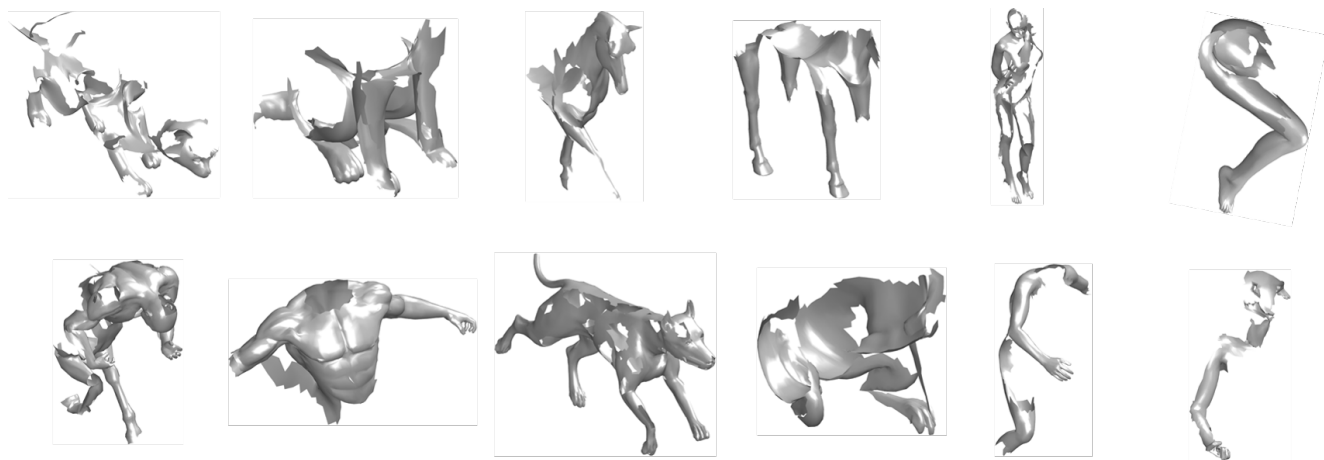


Figure 10. Some examples of cuts and their matching similarity score maps. The compared point is marked in yellow on the cut, whereas ground truth polygon is marked in green, symmetrical polygon in purple, and top 5 matches in grayscale

1296 1350  
1297 1351  
1298 1352  
1299 1353  
1300 1354  
1301 1355  
1302 1356  
1303 1357  
1304 1358  
1305 1359  
1306 1360  
1307 1361  
1308 1362  
1309 1363  
1310 1364  
1311 1365  
1312 1366  
1313 1367  
1314 1368  
1315 1369  
1316 1370  
1317 1371  
1318 1372  
1319 1373  
1320 1374  
1321 1375  
1322 1376  
1323 1377  
1324 1378  
1325 1379  
1326 1380  
1327 1381  
1328 1382  
1329 1383  
1330 1384  
1331 1385  
1332 1386  
1333 1387  
1334 1388  
1335 1389  
1336 1390  
1337 1391  
1338 1392  
1339 1393  
1340 1394  
1341 1395  
1342 1396  
1343 1397  
1344 1398  
1345 1399  
1346 1400  
1347 1401  
1348 1402  
1349 1403

1404  
1405  
1406  
1407  
1408  
1409  
1410  
1411  
1412  
1413  
1414  
1415  
1416  
1417  
1418  
1419  
14201421  
1422  
1423  
1424  
1425  
1426  
1427  
1428  
1429  
1430  
1431  
1432  
1433  
1434  
1435  
1436  
1437  
1438  
1439  
1440  
1441  
1442  
1443  
1444  
1445  
1446  
1447  
1448  
1449  
1450  
1451  
1452  
1453  
1454  
1455  
1456  
1457  
1458  
1459  
1460  
1461  
1462  
1463  
1464  
1465  
1466  
1467  
1468  
1469  
1470  
1471  
1472  
1473  
1474  
1475  
1476  
1477  
1478  
1479  
1480  
1481  
1482  
1483  
1484  
1485  
1486  
1487  
1488  
1489  
1490  
1491  
1492  
1493  
1494  
1495  
1496  
1497  
1498  
1499  
1500  
1501  
1502  
1503  
1504  
1505  
1506  
1507  
1508  
1509  
1510  
15111458  
1459  
1460  
1461  
1462  
1463  
1464  
1465  
1466  
1467  
1468  
1469  
1470  
1471  
1472  
1473  
1474  
1475  
1476  
1477  
1478  
1479  
1480  
1481  
1482  
1483  
1484  
1485  
1486  
1487  
1488  
1489  
1490  
1491  
1492  
1493  
1494  
1495  
1496  
1497  
1498  
1499  
1500  
1501  
1502  
1503  
1504  
1505  
1506  
1507  
1508  
1509  
1510  
1511

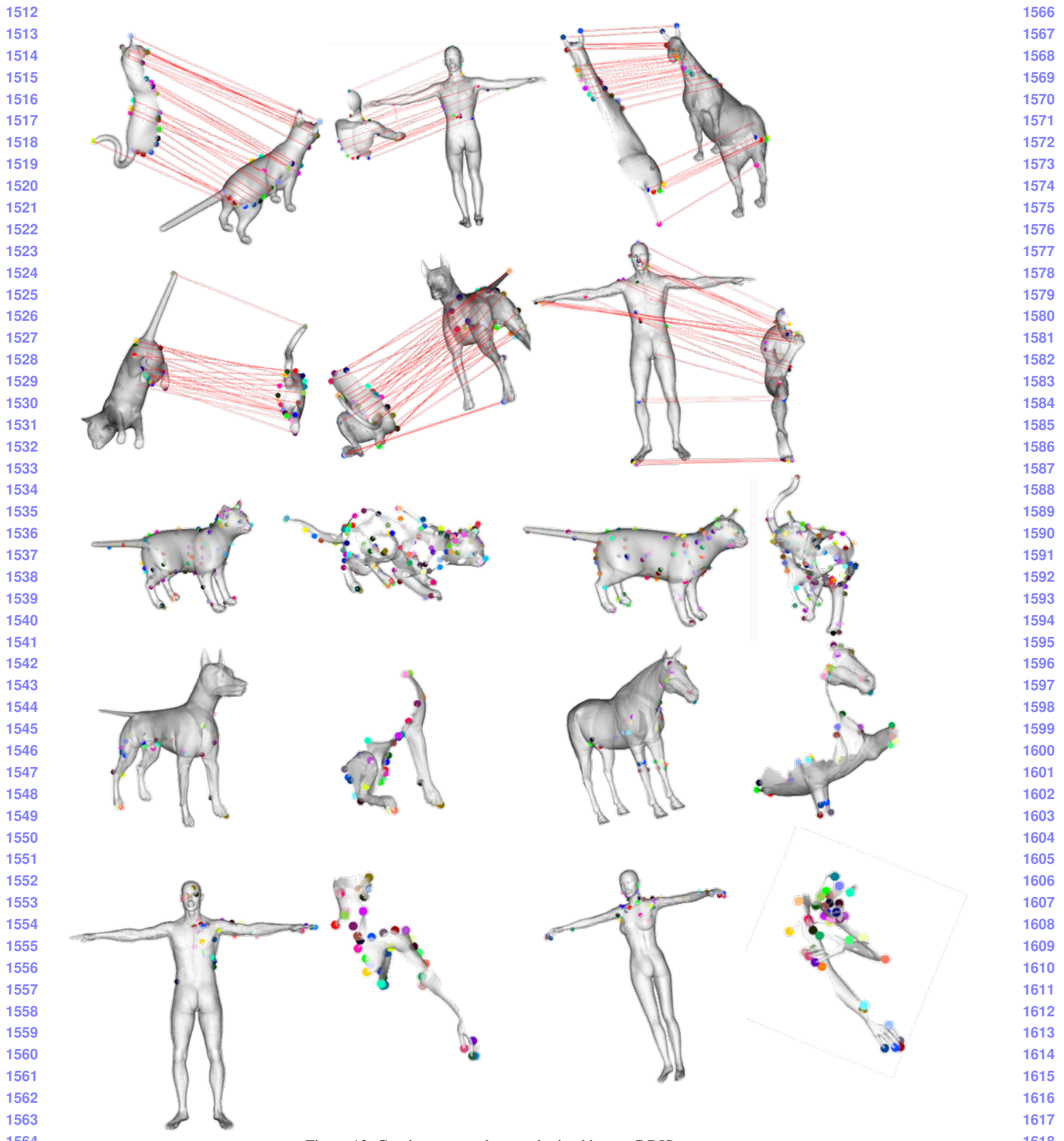


Figure 13. Good correspondences obtained by our DDIS measure

1620  
1621  
1622  
1623  
1624  
1625  
1626  
1627  
1628  
1629  
1630  
1631  
1632  
1633  
1634  
1635  
1636  
1637  
1638  
1639  
1640  
1641  
1642  
1643  
1644  
1645  
1646  
1647  
1648  
1649  
1650  
1651  
1652  
1653  
1654  
1655  
1656  
1657  
1658  
1659  
1660  
1661  
1662  
1663  
1664  
1665  
1666  
1667  
1668  
1669  
1670  
1671  
1672  
1673

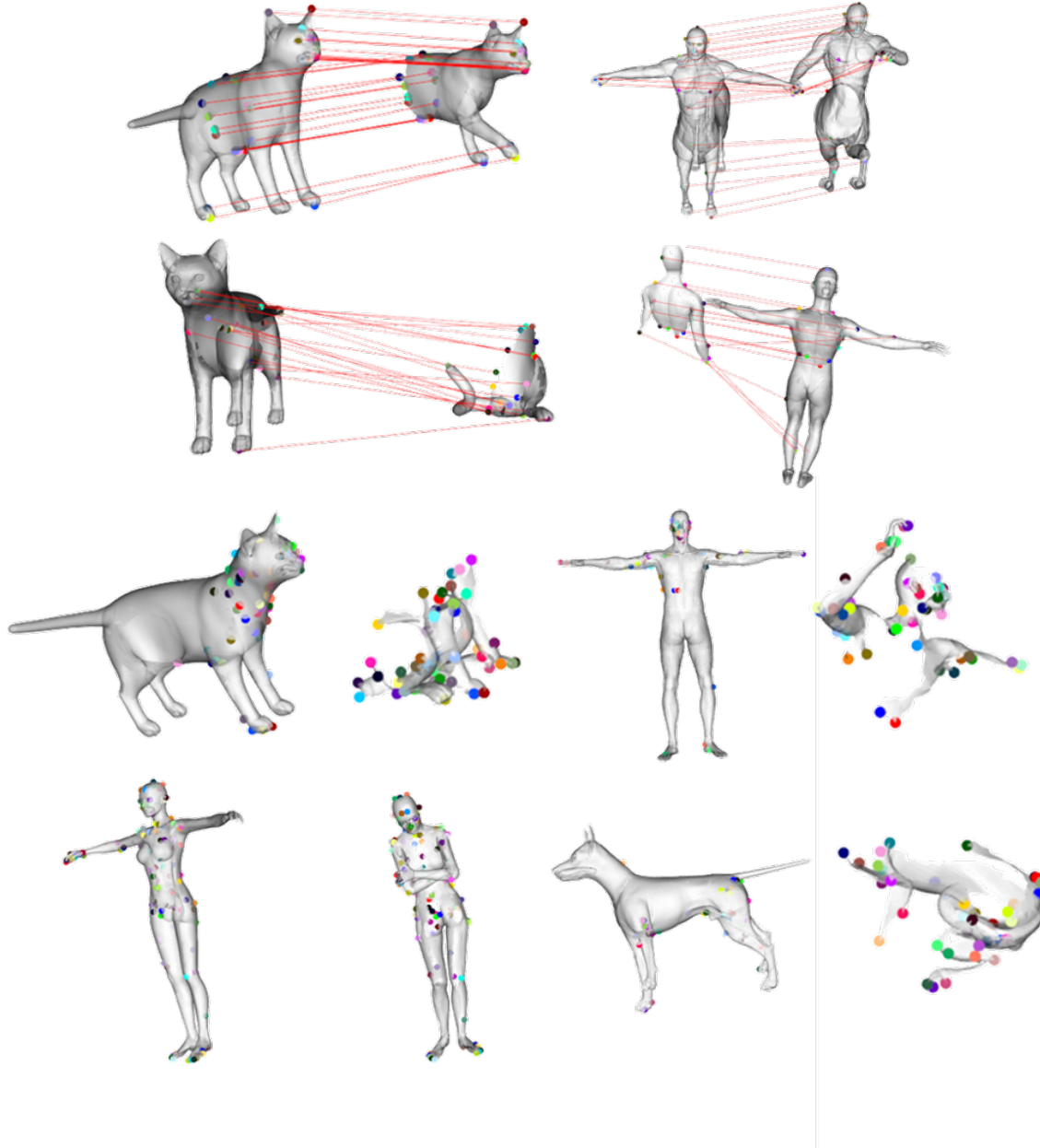


Figure 14. Some notable failure cases - most common is cat paw assignment - an extrinsic near symmetry gives rise to this phenomena. Closed fists on humanoids tends to cause a collapse of all fingers to a single finger. In the holes extreme partiality makes the geodesic distances break even over short distances.

1674  
1675  
1676  
1677  
1678  
1679  
1680  
1681  
1682  
1683  
1684  
1685  
1686  
1687  
1688  
1689  
1690  
1691  
1692  
1693  
1694  
1695  
1696  
1697  
1698  
1699  
1700  
1701  
1702  
1703  
1704  
1705  
1706  
1707  
1708  
1709  
1710  
1711  
1712  
1713  
1714  
1715  
1716  
1717  
1718  
1719  
1720  
1721  
1722  
1723  
1724  
1725  
1726  
1727